

# Partially Nonergodic Empirical Ground-Motion Models for Predicting Horizontal and Vertical PGV, PGA, and 5% Damped Linear Acceleration Response Spectra Using Data from the Iranian Plateau

by Farhad Sedaghati and Shahram Pezeshk

**Abstract** We present new ground-motion prediction equations (GMPEs) to estimate horizontal and vertical strong ground motion intensity measures (GMIMs) generated by shallow active crustal earthquakes occurring within the Iranian plateau. To this end, a dataset containing 688 records from 152 earthquakes with moment magnitudes ranging from 4.7 to 7.4 and Joyner–Boore distances up to 250 km has been used. The effects of the local site condition are taken into account using the time-averaged shear-wave velocities in the upper 30 m ( $V_{S30}$ ). We decided not to include the style-of-faulting term in the final functional form because the total standard deviation is reduced 10% by removing this term from the functional form. We used a nonlinear mixed-effects regression to determine the coefficients of the functional form and to separate out the between-event and between-station standard deviations from the total standard deviation. Significant standard deviation of site-to-site variability demonstrates that the ergodic assumption is not able to account for the spatial variability of ground motions. We introduced random-effects coefficients to capture regional variations between different tectonic regions of the Iranian plateau, such as Alborz and Zagros, in the regression analysis to investigate the effects of regionalization on GMPEs. The results showed that, although the effects of regional variations for considered regions are negligible at close distances, they are significant at longer distances. The complexity and performance of the final functional form is justified by comparing Akaike and Bayesian information criteria values over many trial functional forms. Moreover, the distribution of between-event, site-to-site, and event-station corrected residuals demonstrates that no trends are evident, implying satisfactory performance of the proposed GMPEs. Therefore, the derived GMPEs can be employed to predict GMIMs and to do seismic-hazard assessments within the Iranian plateau.

*Electronic Supplement:* Lists of the events and stations considered in the final dataset and derived coefficients of the functional form.

## Introduction

The Iranian plateau, situated in the middle of the Alpine-Himalayan orogenic belt and characterized by active strike-slip and reverse faults and frequent moderate-to-large earthquakes, is one of the foremost tectonically active areas in the world (Berberian and Yeats, 1999; Tavakoli and Ghafory-Ashtiany, 1999; Ansari and Amini Hosseini, 2014). The Alpine-Himalayan orogenic belt located between the Arabian and Eurasian plates undergoes compressional stresses. This area is considered as a convergent plate tectonic setting. The convergence is still active in a nearly north–south direction at a rate of  $\sim 25$ – $30$  mm/year at the

eastern edge of the Arabian plate (Sella *et al.*, 2002). Even though there is no historical evidence that an earthquake with a magnitude larger than 8 has struck Iran, there is a potential to have a devastating earthquake because no large earthquake has been reported for several long strike-slip faults such as Doruneh and Nayband (Berberian and Yeats, 1999). Therefore, it is vital to be prepared for such a destructive event.

Ghasemi *et al.* (2008), Mousavi *et al.* (2012), and Zafarani and Mousavi (2014), using the ranking schemes proposed by Scherbaum *et al.* (2004, 2009), showed that ground-motion prediction equations (GMPEs) developed

Table 1  
Summary of the Database Ranges and Functional Forms of Ground-Motion Prediction Equations Developed for Iran

	N05	GZFK09	SKTM12	KAAH15	This Study
Region	Iran	Iran and West Eurasia	Iran	Iran	Iran
Number of events	45	200	78	138	152
Number of recordings	279	893	351	528	688
Magnitude scale	Different scales	<b>M</b>	<b>M</b>	<b>M</b>	<b>M</b>
Magnitude range	3.0–7.4	5.0–7.4	5.0–7.3	4.2–7.4	4.7–7.4
Distance scale	$R_{EPI}$	$R_{EPI}$	$R_{RUP}$ and $R_{HYP}$	$R_{JB}$	$R_{JB}$
Maximum distance (km)	245	340	135	200	250
Hinge magnitude	Not used	Not used	Not used	Included	Included
Geometrical spreading term	Included	Included	Included	Included	Included
Anelastic attenuation term	Not used	Not used	Not used	Included	Included
Soil response term	Linear	Linear	Linear	Nonlinear	Linear
Fault mechanism term	Not used	Not used	SS, RV	SS, RV	Not used
Regional variability	Not used	Not used	Not used	Not used	Included
Standard deviation	$\sigma$	$\sigma$	$\tau, \phi, \sigma$	$\tau, \phi, \sigma$	$\tau, \phi_0, \phi_{S2S}, \sigma$
Direction	Horizontal and vertical	Horizontal	Horizontal	Horizontal	Horizontal and vertical
Component of horizontal	SRSM	GMRotI50	Geometric mean	Geometric mean	Geometric mean
GMIM	PGA	PSA	PGV, PGA, and PSA	PGV, PGA, and PSA	PGV, PGA, and PSA

N05, Nowroozi (2005); GZFK09, Ghasemi *et al.*, (2009); SKTM12, Saffari *et al.*, (2012); KAAH15, Kale *et al.*, (2015);  $R_{EPI}$ , epicentral distance;  $R_{RUP}$ , rupture distance;  $R_{HYP}$ , hypocentral distance;  $R_{JB}$ , Joyner–Boore distance;  $\sigma$ , total standard deviation;  $\tau$ , between-event standard deviation;  $\phi$ , within-event standard deviation;  $\phi_0$ , event-site corrected standard deviation;  $\phi_{S2S}$ , site-to-site standard deviation; SRSM, square root of sum of squares of the two components; GMRotI50, 50th percentile of the set of geometric means for a given oscillator period (Boore *et al.*, 2006); PGV, peak ground velocity; PGA, peak ground acceleration; PSA, pseudoabsolute response spectral acceleration; SS, strike-slip; RV, reverse; GMIM, ground motion intensity measures.

based on local databases of different parts of Iran are mostly assigned better ranks compared to Next Generation Attenuation–West (NGA–West) GMPEs. Furthermore, regardless of having a suitable strong-motion network in the country, there is a limited and small number of appropriate and reliable GMPEs based on a local database in which all influential estimator parameters, such as magnitude, distance, site classification, and style-of-faulting, are taken into account. Within the last decade, several empirical GMPEs have been developed to predict ground motion intensity measures (GMIMs) for Iran or a particular region inside the Iranian plateau (e.g., Nowroozi, 2005; Zare and Sabzali, 2006; Ghodrati Amiri *et al.*, 2007, 2010; Ghasemi *et al.*, 2009; Sadeghi *et al.*, 2010; Hamzehloo and Mahood, 2012; Saffari *et al.*, 2012; Kale *et al.*, 2015; Soghrat and Ziyaeifar, 2016). We selected models that have been calibrated based on the data from the whole Iranian plateau and refer to these GMPEs as N05 (Nowroozi, 2005), GZFK09 (Ghasemi *et al.*, 2009), SKTM12 (Saffari *et al.*, 2012), and KAAH15 (Kale *et al.*, 2015). These GMPEs used vastly different approaches and parameters. Table 1 compares their magnitude–distance range of applicability and technical differences, such as terms used in their functional forms.

Epistemic uncertainties are typically captured with a combination of GMPEs using the logic-tree approach, whereas the aleatory uncertainty  $\sigma$  is directly used in the probabilistic seismic-hazard assessment (PSHA) integrations to estimate hazard in a given site, and a small decrease in  $\sigma$  can result in a significant influence on the hazard assessments (Rodriguez-Marek *et al.*, 2014). Therefore, separating out the epistemic uncertainty from the aleatory uncertainty to reduce  $\sigma$  is vital for the new generation of GMPEs. One way to reduce the total

standard deviation is to utilize the partially nonergodic approach (Anderson and Brune, 1999; Rodriguez-Marek *et al.*, 2014; Kotha *et al.*, 2016) in which the site-to-site variability is removed from the total variability. The corrected standard deviation  $\sigma_{SS}$  is known as the single-station sigma (Atkinson, 2006). Another way to reduce the total aleatory standard deviation is to consider the effects of regional differences associated with source, path, and site functions (Stafford, 2014), because databases used to develop GMPEs can be composed of records from different tectonic regions.

Moving toward conducting partially nonergodic region-specific PSHA (Kotha *et al.*, 2017), there is an essential need to update GMPEs derived based on the database of Iranian ground-motion records. In this study, we present new GMPEs to predict the horizontal and the vertical peak ground velocity (PGV), peak ground acceleration (PGA), and 5% damped linear elastic pseudoabsolute response spectral acceleration (PSA) ordinates. Although the functional form seems relatively simple, it captures the main characteristics of ground motions. We used a nonlinear mixed-effects regression analysis discussed by Stafford (2014) instead of the traditional mixed-effects algorithm developed by Abrahamson and Youngs (1992) to partition the total residual into three components (between-event, between-station, and event-site corrected residuals; Chen and Tsai, 2002) and to incorporate random-effects coefficients to account for regional differences among various tectonic regions of the Iranian plateau.

#### Database and Data Processing

The Iranian plateau is composed of many minor seismic zones; however, it is generally divided into two major seis-

mic zones with different tectonic characteristics known as the Alborz and Zagros regions. Records from the Zagros active folded belt generally have distinct frequency content, duration, and attenuation rate compared to records from the Alborz region. Further, the surface structure of these two regions is different (Berberian and Mohajer Ashjai, 1977). As a consequence, the combination of records from these regions with various seismic characteristics and discrepant tectonic settings may result in increased standard deviations of the GMPEs (Douglas, 2004a,b). On the other hand, compilation of a large database aims to improve the range of applicability of the database in terms of magnitude, distance, and site conditions, in addition to deriving reliable and robust GMPEs through the variability of ground motions (Kotha *et al.*, 2016). Ghasemi *et al.* (2009) and Sedaghati and Pezeshk (2016a), utilizing the analysis of variance technique (Douglas, 2004a,b), investigated the regional differences between major seismic zones of Iran and demonstrated that records from the Alborz region can be merged with records from the Zagros region to derive GMPEs, although these regions have different seismic characteristics. In this article, we use a dataset containing records from different tectonic regions of Iran (Alborz, Zagros, and others) to have a wider magnitude–distance range of applicability of the derived GMPEs to be used within PSHA. Thus, random-effects coefficients in the functional form are introduced to explore the effects of regional variations on GMPEs.

We collected uncorrected triaxial accelerograms for this study from the Iranian Strong Motion Network (ISMN) data recorded by the Building and Housing Research Center of Iran. The ISMN recording sensors include both analog instruments, the kinematics SMA-1 that is an optical-mechanical device and digital instruments SSA-2. Waveforms used in this study occurred during the period of 1979–2013. These records have been visually inspected, and poor quality data have been removed. To avoid confronting any biases, we performed a baseline adjustment, including subtracting the mean from the raw waveform and removing the linear trend. Then, the response of the instruments has been deconvolved with the recorded signals to correct for the instrument response. The next step is to deal with noise, which can have obvious and significant impacts on the velocity and displacement time histories obtained by the integration of an acceleration time history. It should be mentioned that, even though the separation of the noise from the signal is impossible, data processing and filtering can aid an analyst to identify which part of the signal has satisfactory signal-to-noise ratio (SNR) to be used for further investigations and to remove the part of the signal which is heavily contaminated by noise (Boore and Bommer, 2005; Douglas and Boore, 2011). Therefore, a phaseless eight-pole band-pass filter has been applied on every single zero-padded accelerogram to remove portions of accelerograms for which SNRs are unacceptable. To prevent distortion of the size and location of the peaks in waveforms, a phaseless (acausal) filter is used to filter signals, because causal filters may change the phase portion of

signals. Filter cutoff frequencies for each accelerogram are very important and can easily change values of PGV, PGA, and PSAs (Akkar and Bommer, 2006, 2007). To determine these cutoff frequencies, the Fourier amplitude of the signal to the Fourier amplitude of the noise plot has been used, in which the signal is defined as a window after the origin time and the noise is defined as a window before the origin time. The length of this window is variable and flexible based on the pre-event length of the record. The lower and upper cutoff frequencies are frequencies at which the Fourier amplitude of the signal to the Fourier amplitude of the noise becomes less than three (Akkar and Bommer, 2006; Ghasemi *et al.*, 2009). After processing the initial database, we applied the following criteria to create the final dataset to perform regression:

- Records lacking the three components are discarded from the final dataset.
- Because the proposed GMPEs are developed for shallow active crustal earthquakes, we consider events with focal depths less than 35 km to be included in the final dataset.
- Only records with Joyner–Boore distances less than 250 km are included in the final dataset.
- Records with unknown  $V_{S30}$  are excluded from the final dataset. It should be mentioned that 30% of the data in the initial database had no  $V_{S30}$ , and they are eliminated from the final dataset.
- Regarding the recent attention about accounting for the effects of small magnitude events within PSHA (Bindi *et al.*, 2014), we did not set any limitations for the moment magnitude. However, our initial database consists of records with a minimum moment magnitude of 4.7.

The final dataset is composed of 688 records out of 152 earthquakes recorded at 321 different stations, with moment magnitudes varying from 4.7 to 7.4 and Joyner–Boore distances within 250 km. This dataset has 46 singly recorded earthquakes. We kept singly recorded earthquakes and aftershocks in the final dataset if they passed the above-mentioned criteria. Figure 1 demonstrates the locations of the considered stations as well as the locations of the selected earthquakes. Figure 2 illustrates the distribution of data in the magnitude–distance space. It should be noted that the number of records with distances less than 10 km is not adequately robust; hence, the predicted median ground motions may not be well constrained at very short distances. Out of 688 records, 262 records are from the Zagros region, 132 records are from the Alborz region, and 294 records are from other regions, such as central and eastern Iran. Histograms of the selected records with respect to magnitude, distance, and  $V_{S30}$  for each region are displayed in Figure 3. Table S1 (available in the electronic supplement to this article) lists all the earthquakes, dates, times, epicentral longitudes and latitudes, moment magnitudes, depths, and the number of records for each

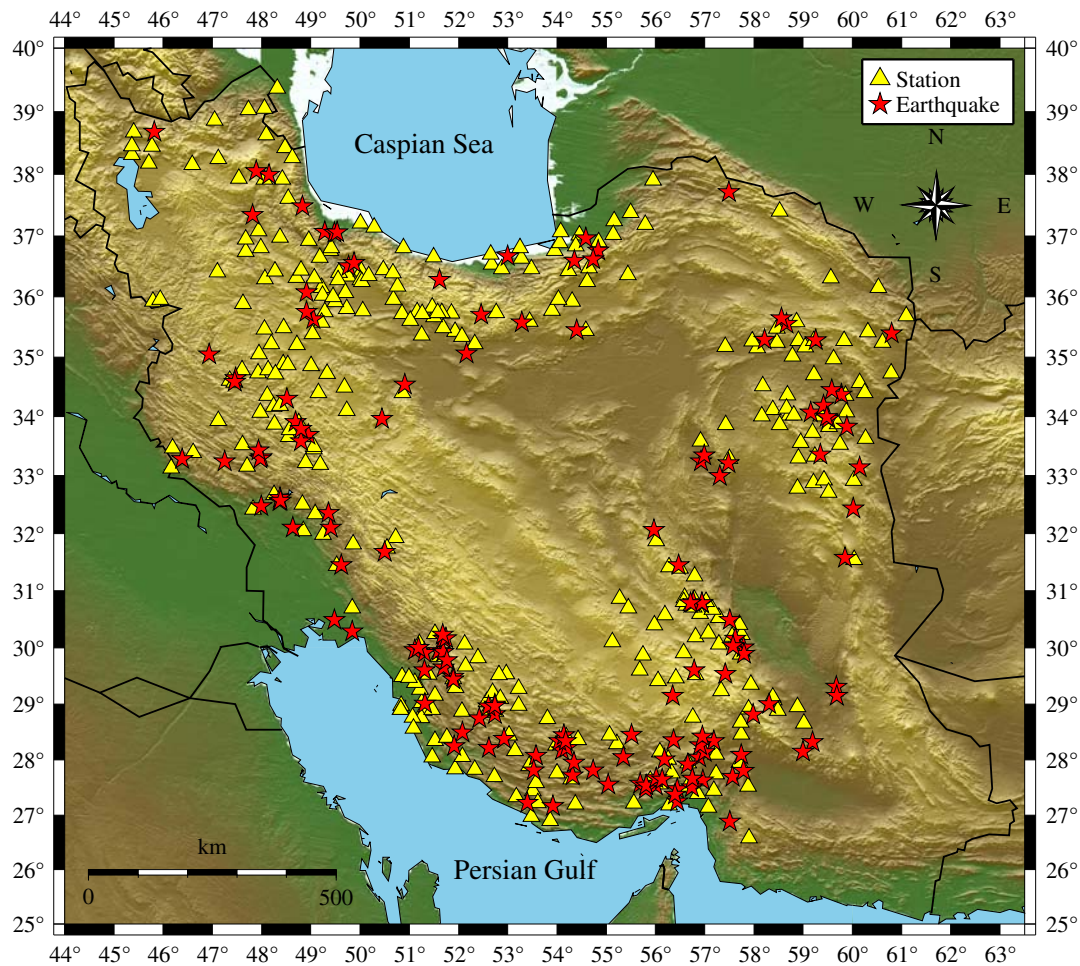


**Figure 1.** Locations of the considered stations and selected earthquakes. The color version of this figure is available only in the electronic edition.

earthquake considered in the final dataset. Table S2 lists the name of stations, their longitudes and latitudes,  $V_{530}$ , and the number of records for each station.

The vertical component and the geometric mean of the horizontal components for PGV, PGA, and PSA ordinates are considered as the vertical and the horizontal GMIMs of interest, respectively. Niazi and Bozorgnia (1991), Elnashai and Papazoglou (1997), Ambraseys and Douglas (2003), and Bozorgnia and Campbell (2004) discussed the effect of vertical ground motions on structures that should be taken into account, particularly for near-source distances; therefore, we estimated the coefficients of the functional form for the vertical component as well as the horizontal component. We considered 13 spectral periods: 0.050, 0.075, 0.10, 0.15, 0.20, 0.30, 0.50, 0.75, 1.0, 1.5, 2.0, 3.0, and 4.0 s. We restricted the spectral periods to these values because the number of records out of this range is very small, and the regression analysis does not yield a robust result. The peak ground displacement is intensively sensitive to the cutoff frequencies of the applied band-pass filter; therefore, this GMIM is not considered in the developed GMPEs (Boore *et al.*, 2014).

### Functional Form and Regression Method

Kaklamanos and Baise (2011) compared various NGA-West GMPEs and demonstrated that sophisticated functional forms essentially do not guarantee more accuracy and reduction of their standard deviations compared to simple functional forms. Hence, we included terms corresponding to the predictor variables that are available in the database. Kotha *et al.* (2016) used the same functional form proposed by Bindi *et al.* (2014) for Europe and the Middle East and showed that incorporating regional variations as random effects in the functional form results in a significant decrease in the total aleatory standard deviation. In this study, we use a parametric regression approach in which coefficients are calibrated using the nonlinear mixed-effects algorithm and consider the presence of regional variations in ground motions. In this regard, we use the nonlinear mixed-effects regression algorithm developed by Lindstrom and Bates (1990) and exerted in MATLAB with the functions of nlmeFit and fitlmeMatrix (MathWorks Inc., 2015).

Generally, observed ground motions are a function of source, path, and site effects. To develop a framework for

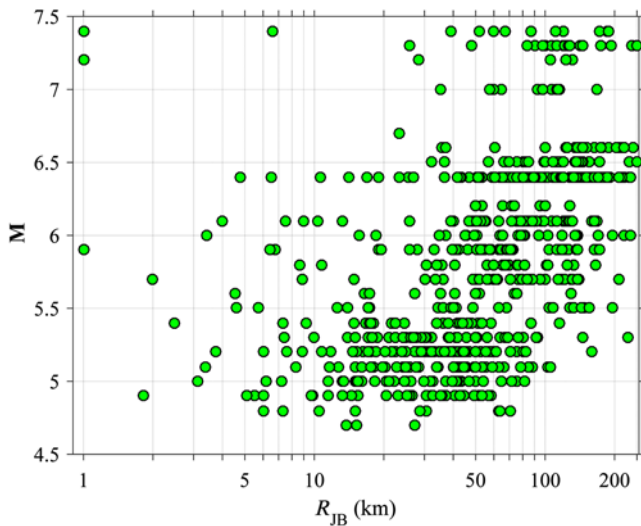


**Figure 2.** Distribution of the considered data in the magnitude–distance space. Records with  $R_{JB}$  (Joyner–Boore distance) less than 1 km are demonstrated at 1 km in the plots. The color version of this figure is available only in the electronic edition.

the functional form, the first step is inspecting nonparametric plots of data, such as PSA values versus distance, to explore the magnitude and distance dependence of PGA and PSA ordinates. Sedaghati and Pezeshk (2016b) showed that selecting an appropriate functional form is the main step to calibrating GMPEs, whereas the effect of choosing a specific regression procedure to derive the model coefficients is insignificant. Accordingly, we chose many trial functional forms with distinctive terms included, and compared Akaike and Bayesian information criteria (AIC and BIC, respectively) values and the logarithms of their likelihoods to find an appropriate functional form that can best fit the data. Based on the considerations discussed, we propose the following functional form

$$\ln(Y) = f_{\text{source}} + f_{\text{path}} + \delta B_e + \delta W, \quad (1)$$

in which

$$\delta W = f_{\text{site}} + \delta_{S2S} + \varepsilon, \quad (2)$$

and  $\ln(Y)$  is the natural logarithm of the GMIM of interest (PGA and PSAs in  $g$  and PGV in  $\text{cm/s}$ ),  $\delta W$  is the within-event term, and  $\delta B_e$  and  $\delta_{S2S}$  are the random effects in the models to describe the between-event and site-to-site residuals.  $\delta B_e$  has a normal distribution with zero mean and standard deviation of  $\tau$ .  $\delta_{S2S}$  has a normal distribution with zero mean and standard deviation of  $\phi_{S2S}$  (Al Atik *et al.*, 2010).  $\varepsilon$  is the event-site corrected residual having normal distribution with zero mean and standard deviation of  $\phi_0$ .  $f_{\text{source}}$ ,  $f_{\text{path}}$ , and  $f_{\text{site}}$  are the source, the path, and the site functions, respectively.

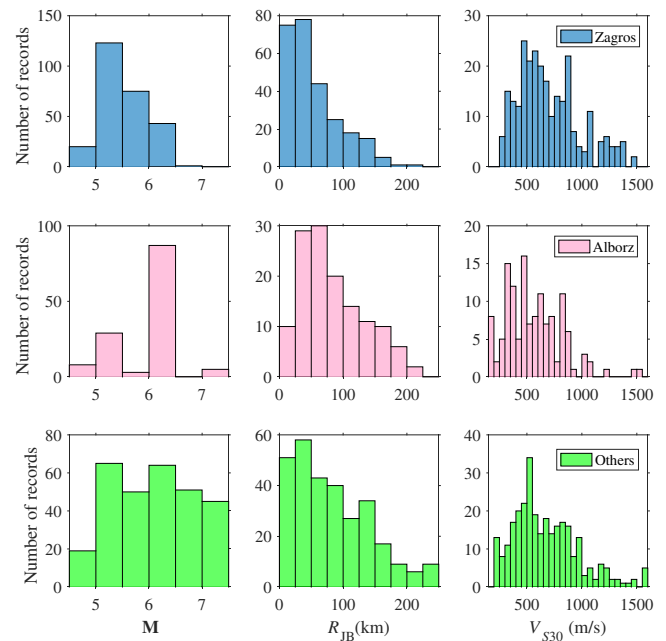


**Figure 3.** Histograms demonstrating the distribution of the data used with respect to magnitude, distance, and  $V_{S30}$  for each group. The color version of this figure is available only in the electronic edition.

The source function is given by

$$f_{\text{source}} = \begin{cases} a_1 + a_2(\mathbf{M} - \mathbf{M}_h) + a_3(\mathbf{M} - \mathbf{M}_h)^2 & \mathbf{M} \leq \mathbf{M}_h \\ a_1 + a_4(\mathbf{M} - \mathbf{M}_h) & \mathbf{M} > \mathbf{M}_h \end{cases}, \quad (3)$$

in which  $\mathbf{M}$  is the moment magnitude,  $\mathbf{M}_h$  is the hinge magnitude fixed at 7.0, and  $a_1$  to  $a_4$  are fixed-effects coefficients. The coefficient  $a_4$ , which represents the saturation effect with magnitude, is not constrained to be nonnegative to allow capturing the oversaturation effect with magnitude if it exists in the dataset.

The path function describing the effects of the geometrical spreading, the magnitude-dependent geometrical spreading, and the anelastic attenuation (Sedaghati and Pezeshk, 2016c) is defined as

$$f_{\text{path}} = (b_1 + b_2\mathbf{M}) \ln(\sqrt{R_{JB}^2 + h^2}) + (b_3 + \Delta b_{3,\text{region}})(\sqrt{R_{JB}^2 + h^2}), \quad (4)$$

in which  $R_{JB}$  is the Joyner–Boore distance,  $b_1$ ,  $b_2$ ,  $b_3$ , and  $h$  (fictitious depth) are fixed-effects coefficients, and  $\Delta b_3$  is a random-effect coefficient to capture the effects of regional variations in the anelastic attenuation ( $Q^{-1}$ ). Since there is a trade-off between the geometric spreading and the anelastic attenuation terms because of the scatter of data, we restricted the coefficient  $b_3$  to be negative or zero.

Table 2  
Derived Source, Path, and Site-Effects Coefficients of the Functional Form for the Horizontal Component

Period	$a_1$	$a_2$	$a_3$	$a_4$	$b_1$	$b_2$	$b_3$	$h$	$c_1$	$c_2$
PGV	4.33325	1.41553	0.05836	0.86556	-0.01452	-0.09448	0.00000	3.43732	1.04360	-0.16201
PGA	0.44780	0.24582	-0.14444	0.49645	-1.17792	0.04959	0.00000	4.52478	0.68185	-0.10727
0.050	1.28296	0.39084	-0.06956	0.41181	-1.26192	0.03221	0.00000	5.57414	-0.14576	0.02251
0.075	1.79752	0.40895	-0.07594	0.48121	-1.21353	0.01317	0.00000	6.69748	-0.41950	0.06567
0.10	1.75732	0.44831	-0.10471	0.51506	-0.91959	-0.01771	-0.00132	5.89668	-0.23816	0.03735
0.15	1.92211	0.68712	-0.09073	0.42364	-0.66230	-0.05142	-0.00107	5.05776	0.53382	-0.08402
0.20	1.84094	0.81142	-0.06014	0.41682	-0.61504	-0.05301	-0.00052	5.21685	0.96326	-0.15205
0.30	0.93871	0.42956	-0.12175	-0.13730	-1.08613	0.04596	-0.00141	4.05788	1.94902	-0.30571
0.50	0.16310	0.12164	-0.25975	0.15371	-1.26131	0.08491	-0.00131	4.79965	2.41536	-0.37835
0.75	-0.35304	0.07930	-0.27238	0.49447	-1.45150	0.11993	-0.00114	6.58682	2.32740	-0.36478
1.0	-0.32946	0.09923	-0.31769	0.33462	-1.53799	0.11986	0.00000	9.71673	2.31834	-0.36319
1.5	-1.07387	0.17559	-0.31747	0.32466	-1.69699	0.15532	0.00000	8.85002	2.65348	-0.41564
2.0	-1.34555	0.21828	-0.33131	0.39197	-1.86417	0.17975	0.00000	10.79563	2.61514	-0.40933
3.0	-1.71058	0.18318	-0.40189	0.60346	-2.02030	0.20208	0.00000	14.60791	2.32699	-0.36371
4.0	-1.64664	0.42652	-0.33922	0.66777	-2.06789	0.20052	0.00000	20.18967	2.01555	-0.31493

PGA and PSAs are in units of  $g$ , and PGV has units of  $\text{cm/s}$ .

The site function describing the effects of the near-surface site diminution  $\kappa_0$  (Anderson and Hough, 1984) and the site amplification is defined as

$$f_{\text{site}} = c_1 + c_2 \ln(V_{S30}), \quad (5)$$

in which  $c_1$  and  $c_2$  are fixed-effects coefficients. We did not account for the nonlinear site amplification effects because our dataset is deficient in records with high moment magnitude and very short Joyner–Boore distance captured at stations with low  $V_{S30}$ .

It is worth mentioning that we first introduced random effects on all fixed-effects coefficients, particularly on  $c_1$  and  $c_2$ , to capture the effects of regional differences in  $\kappa_0$  and site amplification in trial functional forms. However, based on the performance of those functional forms and comparing the  $p$ -value of each random-effects coefficient, explaining the significance of that coefficient in the functional form and AIC and BIC values, we decided to represent the anelastic attenuation term by both fixed-effects and random-effects coefficients and to disregard the remaining random-effects coefficients.

Furthermore, in our trial functional forms, we first incorporated coefficients corresponding to the style-of-faulting term; yet,  $p$ -values of those coefficients reveal that they are statistically insignificant. Removing the style-of-faulting term from the functional form reduced the total standard deviation of residual by 10%. At most periods, the between-station standard deviation is nearly constant with or without the style-of-faulting term; yet, the between-event and event-site corrected standard deviations are reduced after disregarding the style-of-faulting term. Thus, following Kotha *et al.* (2016), we decided to eliminate the style-of-faulting term from the final functional form.

Because of rising interest in implementing site-specific PSHA (Kotha *et al.*, 2017), we performed the regression analysis in two steps (equations 1 and 2) to separate out the site-to-

site component  $\delta_{S2S}$  from the total residual. As a consequence, the site-corrected standard deviation can be obtained from

$$\sigma_0 = \sqrt{\tau^2 + \phi_0^2}. \quad (6)$$

Then,  $\delta_{S2S} \pm \text{SE}$  (standard error) is modeled as the site-adjustment factor and its epistemic uncertainty (Rodriguez-Marek *et al.*, 2014). On the other hand, in traditional PSHA (i.e., ergodic assumption), all residual components are considered to obtain the total aleatory uncertainty

$$\sigma = \sqrt{\tau^2 + \phi_0^2 + \phi_{S2S}^2}. \quad (7)$$

## Results and Discussion

We first performed the mixed-effects regression analysis on equation (1) to obtain the source and path effects coefficients. Then, we performed another mixed-effects regression analysis on equation (2) using the within-event residuals obtained from the first stage to acquire the coefficients of the site-effects term. The source, path, and site-effects coefficients are listed in Tables 2 and 3 for the horizontal and vertical directions, respectively. Associated standard deviations and regional variations coefficients in anelastic attenuation terms are tabulated in Tables 4 and 5 for the horizontal and vertical directions, respectively. We also provided these tables as [E](#) Tables S3–S6. Moreover, site-to-site residuals for all stations to be used in site-specific PSHA studies are provided as [E](#) Tables S7 and S8 for horizontal and vertical directions, respectively.

Figure 4 compares the horizontal and vertical anelastic attenuation coefficients. The effect of the apparent anelastic attenuation is negligible at very low and very high frequency ranges; yet, it is significant in the intermediate frequency range of 1–20 Hz (Atkinson, 2004). An interesting point

Table 3  
Derived Source, Path, and Site-Effects Coefficients of the Functional Form for the Vertical Component

Period	$a_1$	$a_2$	$a_3$	$a_4$	$b_1$	$b_2$	$b_3$	$h$	$c_1$	$c_2$
PGV	3.84553	1.12721	-0.11120	1.12538	0.06376	-0.11459	0.00000	7.33430	0.45063	-0.06904
PGA	-0.32176	0.00795	-0.14011	0.32612	-1.60377	0.12555	-0.00223	4.90710	-0.01229	0.00132
0.050	1.66400	0.24546	-0.10090	0.85470	-1.64838	0.06451	-0.00155	7.46483	-0.93195	0.14539
0.075	1.36236	0.23167	-0.15349	1.00740	-1.29590	0.03809	-0.00405	7.19732	-0.35834	0.05544
0.10	0.82558	0.41494	-0.03751	0.43918	-1.19230	0.05304	-0.00546	4.66372	0.07088	-0.01254
0.15	0.94686	0.56822	-0.07128	0.50286	-0.94059	0.01084	-0.00395	5.06452	0.22220	-0.03549
0.20	1.35291	0.89665	-0.01630	0.15262	-0.78544	-0.03050	-0.00154	6.87616	0.24147	-0.03881
0.30	0.76382	0.56948	-0.06353	0.03079	-1.19802	0.03999	-0.00090	8.98875	0.36840	-0.05870
0.50	-0.38842	-0.28561	-0.31437	0.16822	-1.77938	0.14813	-0.00093	10.32620	0.16614	-0.02711
0.75	-1.08457	-0.89586	-0.40550	-0.00072	-2.56429	0.27182	0.00000	13.27726	0.58054	-0.09177
1.0	-1.15711	-0.71209	-0.38767	-0.23647	-2.56498	0.27067	0.00000	15.46950	0.63574	-0.09969
1.5	-1.67083	-0.94815	-0.45175	-0.25892	-3.09290	0.35369	0.00000	17.64422	0.90997	-0.14213
2.0	-1.70981	-0.46810	-0.38954	-0.28465	-2.83722	0.31440	0.00000	17.49300	1.15554	-0.18050
3.0	-1.31340	0.18260	-0.38439	-0.13375	-2.26790	0.21694	0.00000	23.02558	0.66731	-0.10358
4.0	-0.78427	0.66893	-0.32855	-0.03085	-1.94019	0.14942	0.00000	31.60893	0.81452	-0.12683

PGA and PSAs are in units of  $g$ , and PGV has units of  $cm/s$ .

Table 4  
Associated Standard Deviations of the Proposed Functional Form and Random-Effects Coefficients for the Horizontal Component

Period	$\tau$	$\phi_{S2S}$	$\phi_0$	$\sigma$	$\Delta b_{3,Alborz}$	$\Delta b_{3,Zagros}$	$\Delta b_{3,Others}$	SE ( $\Delta b_{3,Alborz}$ )	SE ( $\Delta b_{3,Zagros}$ )	SE ( $\Delta b_{3,Others}$ )
PGV	0.21991	0.27471	0.56986	0.66975	0.00000	0.00000	0.00000	0.00000	0.00000	0.00000
PGA	0.20592	0.20338	0.45542	0.53961	0.00000	0.00000	0.00000	0.00000	0.00000	0.00000
0.050	0.26759	0.24464	0.52383	0.63706	0.00000	0.00000	0.00000	0.00000	0.00000	0.00000
0.075	0.29109	0.26182	0.51187	0.64443	0.00000	0.00000	0.00000	0.00000	0.00000	0.00000
0.10	0.26870	0.29404	0.53584	0.66767	0.00000	0.00000	0.00000	0.00000	0.00000	0.00000
0.15	0.24067	0.28827	0.53874	0.65671	0.00000	0.00000	0.00000	0.00000	0.00000	0.00000
0.20	0.22902	0.28460	0.53337	0.64648	0.00000	0.00000	0.00000	0.00000	0.00000	0.00000
0.30	0.26071	0.23028	0.56110	0.66018	0.00001	-0.00009	0.00008	0.00007	0.00003	0.00004
0.50	0.23706	0.24270	0.62001	0.70676	0.00007	-0.00018	0.00011	0.00019	0.00044	0.00010
0.75	0.25190	0.30756	0.64693	0.75932	0.00015	-0.00069	0.00054	0.00065	0.00062	0.00065
1.0	0.25511	0.34064	0.65563	0.78164	0.00000	0.00000	0.00000	0.00000	0.00000	0.00000
1.5	0.26505	0.36046	0.68288	0.81640	0.00000	0.00000	0.00000	0.00000	0.00000	0.00000
2.0	0.23501	0.36160	0.68411	0.80870	0.00000	0.00000	0.00000	0.00000	0.00000	0.00000
3.0	0.33210	0.33375	0.63807	0.79298	0.00000	0.00000	0.00000	0.00000	0.00000	0.00000
4.0	0.48985	0.27984	0.60826	0.82960	0.00000	0.00000	0.00000	0.00000	0.00000	0.00000

All standard deviations are in natural logarithm units. SE, standard error.

is that the horizontal anelastic attenuation is weaker than the vertical, due to the higher frequency content of the vertical component compared with the horizontal component (Stewart *et al.*, 2016). Bindi *et al.* (2011) and Stewart *et al.* (2016) also had similar observations comparing the vertical and horizontal anelastic attenuation coefficients.

Figure 5 shows the comparison of the horizontal and vertical  $V_{S30}$ -scaling coefficients. The site response for the vertical component is significantly lower than for the horizontal component. This confirms the assumption of the H/V technique in which the vertical site amplification is negligible compared to the horizontal site amplification to measure the site response (Lermo and Chavez-Garcia, 1993; Zandieh and Pezeshk, 2011). For periods less than about 0.1 s, the  $V_{S30}$ -scaling coefficients are positive. It is very well established that softer sites (lower  $V_{S30}$ ) amplify long-period motions, whereas

stiffer sites (higher  $V_{S30}$ ) amplify short-period motions. Therefore, having positive site-response values at short period is justified. The reader is referred to Kramer (1996) for a discussion of the comparison of the site amplification effects within different sites. A similar observation was made by Ghasemi *et al.* (2009) and Soghrat and Ziyaeifar (2016).

Figure 6 displays the period dependence comparison of the standard deviations. The between-event and site-to-site standard deviations of vertical and horizontal motions are comparable; however, the event-site corrected standard deviation of the vertical component is higher than the horizontal component, resulting in a higher overall standard deviation for the vertical component. Stewart *et al.* (2016) also observed the same trend comparing total standard deviations of vertical and horizontal components. This indicates that there is more scatter of data in the vertical direction than

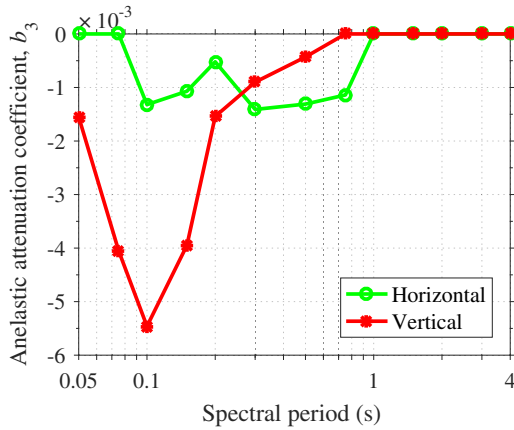


**Figure 4.** Comparison of the horizontal and vertical apparent anelastic attenuation coefficients. The color version of this figure is available only in the electronic edition.

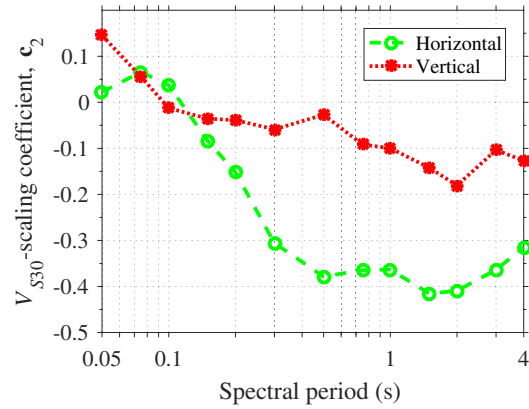


**Figure 5.** Comparison of the horizontal and vertical  $V_{S30}$ -scaling coefficients. The color version of this figure is available only in the electronic edition.

in the horizontal direction. Because we did not discard singly recorded earthquakes or singly recorded stations, the between-event and site-to-site standard deviations may be slightly underestimated.

Figures 7 and 8 show the decay rate (attenuation) of the estimated spectral accelerations with distance for the horizontal and vertical components, respectively. The median distance scaling of the proposed GMPEs are computed for a reference site with  $V_{S30}$  of 760 m/s. We chose PSA at a period of 1.0 s because it is widely used in the seismic-hazard analysis (Tavakoli and Pezeshk, 2005; Rezaeian et al., 2015). The distance attenuation trends show that spectral accelerations are fairly constant (flat) for distances up to 5 km, whereas the decay rates of spectral accelerations are relatively steep for distances more than 10 km. Moreover, the  $M$  scaling, indicating the relative positions of the curves for a specific distance, is weak for high frequency and becomes stronger for low frequencies. In addition, the curvature on

the curves of the vertical component implies the stronger vertical anelastic attenuation compared to the horizontal.

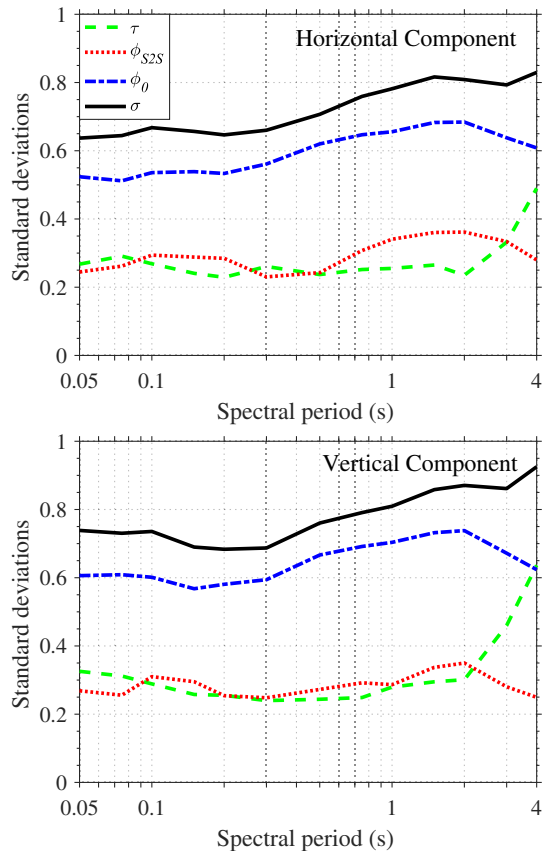
Figures 9 and 10 present the variation of the estimated median response spectra versus spectral period for sites with  $V_{S30}$  of 360 and 760 m/s located at Joyner–Boore distances of 10 and 100 km for horizontal and vertical components, respectively. The comparison of the predicted median response spectra at different distances and magnitudes confirms that the spectral acceleration decreases as distance increases, and increases with increasing magnitude. Furthermore, it can be seen that the predominant period, defined as the period in which the response spectrum is maximum (Boore et al., 2014), systematically increases with increasing moment magnitude for the horizontal component. However, the locations of the predominant period do not noticeably change with magnitude for the vertical component. Bozorgnia and Campbell (2016a) and Stewart et al. (2016) had a similar observation for horizontal and vertical predominant periods.

Table 5

Associated Standard Deviations of the Proposed Functional Form and Random-Effects Coefficients for the Vertical Component

Period	$\tau$	$\phi_{S2S}$	$\phi_0$	$\sigma$	$\Delta b_{3,Alborz}$	$\Delta b_{3,Zagros}$	$\Delta b_{3,Others}$	SE ( $\Delta b_{3,Alborz}$ )	SE ( $\Delta b_{3,Zagros}$ )	SE ( $\Delta b_{3,Others}$ )
PGV	0.27917	0.28996	0.57154	0.69905	0.00000	0.00000	0.00000	0.00000	0.00000	0.00000
PGA	0.21104	0.16597	0.50317	0.57032	0.00000	0.00000	0.00000	0.00000	0.00000	0.00000
0.050	0.32567	0.26859	0.60610	0.73862	0.00000	0.00000	0.00000	0.00000	0.00000	0.00000
0.075	0.31193	0.25567	0.60890	0.73036	0.00000	0.00000	0.00000	0.00000	0.00000	0.00000
0.10	0.28880	0.31005	0.60135	0.73563	0.00000	0.00000	0.00000	0.00000	0.00000	0.00000
0.15	0.25778	0.29522	0.56773	0.68987	0.00000	0.00000	0.00000	0.00000	0.00000	0.00000
0.20	0.25529	0.25430	0.58073	0.68344	0.00007	-0.00025	0.00018	0.00038	0.00037	0.00042
0.30	0.23982	0.24810	0.59422	0.68714	0.00004	-0.00018	0.00015	0.00033	0.00032	0.00033
0.50	0.24370	0.27256	0.66659	0.76028	-0.00049	-0.00042	0.00090	0.00072	0.00069	0.00073
0.75	0.24878	0.29194	0.69164	0.79088	0.00000	0.00000	0.00000	0.00000	0.00000	0.00000
1.0	0.27942	0.28654	0.70367	0.80953	0.00000	0.00000	0.00000	0.00000	0.00000	0.00000
1.5	0.29497	0.33724	0.73200	0.85823	0.00000	0.00000	0.00000	0.00000	0.00000	0.00000
2.0	0.30107	0.34996	0.73815	0.87062	0.00000	0.00000	0.00000	0.00000	0.00000	0.00000
3.0	0.46021	0.28037	0.67186	0.86128	0.00000	0.00000	0.00000	0.00000	0.00000	0.00000
4.0	0.63650	0.24940	0.62358	0.92530	0.00000	0.00000	0.00000	0.00000	0.00000	0.00000

All standard deviations are in natural logarithm units.



**Figure 6.** Comparison of between-event, site-to-site, event-site corrected, and total aleatory standard deviations with respect to spectral period for horizontal and vertical components. The color version of this figure is available only in the electronic edition.

The introduced random-effects term on the anelastic attenuation for each region  $\Delta b_3$  indicates that the effects of regionalization on the anelastic attenuation only show up in the middle frequency range, indicating the fact that the anelastic attenuation effect is negligible at very low and very high frequencies (Aki, 1980). This little variation between the anelastic attenuation in different regions of the Iranian plateau in the middle frequency range is caused either by the difference in the lithosphere structure of these regions or by the difference in scattered heterogeneities within the crust or by the difference of the viscosity of the lithosphere (Sedaghati and Pezeshk, 2016c). The effects of regionalization on the median prediction are demonstrated in Figure 11. The difference between predicted median motions grows with increasing distance because the anelastic attenuation influences the curvature of the distance decay of spectral accelerations. However, there is a negligible difference between predicted median motions for distances less than 100 km, indicating that the impact of the geometric spreading outweighs the anelastic attenuation at close distances, whereas the impact of the anelastic attenuation outweighs the geometric spreading at long distances (Atkinson and Boore, 2014). Figure 12 illustrates the effects of regionalization on the median response spectra for sites at Joyner–Boore

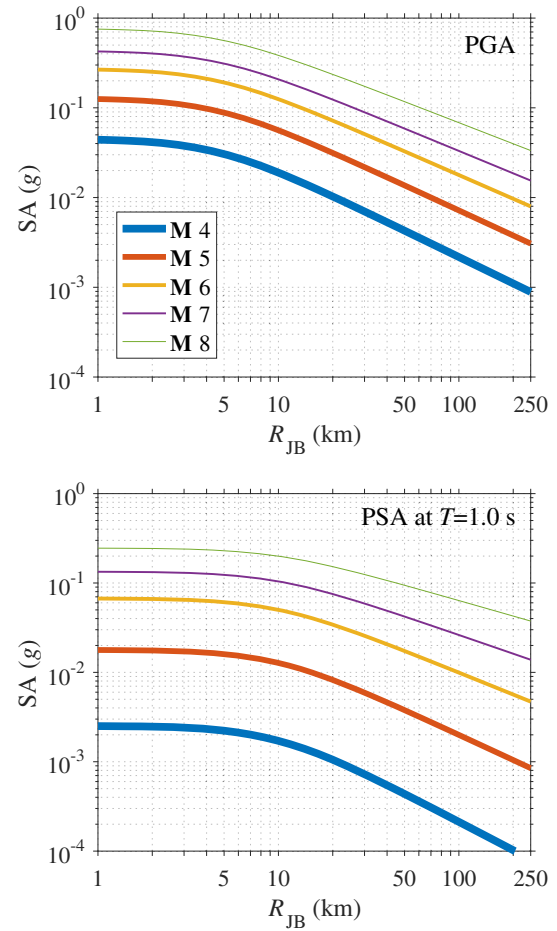


**Figure 7.** Comparison of distance scaling characteristics of our proposed ground-motion prediction equations (GMPEs) for the horizontal component of spectral accelerations (SAs) for a reference site with  $V_{S30} = 760$  m/s. PGA, peak ground acceleration; PSA, pseudoabsolute response spectral acceleration. The color version of this figure is available only in the electronic edition.

distances of 10 and 200 km and  $V_{S30}$  of 760 m/s. For the site at distance of 10 km, regional differences in anelastic attenuation are clearly insignificant, whereas for the site at distance of 200 km, the influence of regional variations on the response spectra is obvious in the intermediate frequency range.

The distribution of between-event, site-to-site, and event-site corrected residuals, respectively, describes the robustness of the source ( $\mathbf{M}$ -scaling), site ( $V_{S30}$ -scaling), and path (distance-scaling) terms of the functional form. Figures 13 and 14 display between-event, site-to-site, and event-site corrected residuals against predictor variables to explore the validity of our median GMPEs for PGA and PSA at a period of 1.0 s for the horizontal and vertical directions, respectively. We used 0.25  $\mathbf{M}$ , 100 m/s, and 25 km interval bins to compute the average values of residuals. Error bars represent the mean of binned residuals along with their 95% confidence intervals. It should be noted that we combined two last magnitude bins because the number of records were few. We considered bins in which there are at least three observations to estimate the mean of binned residuals. The

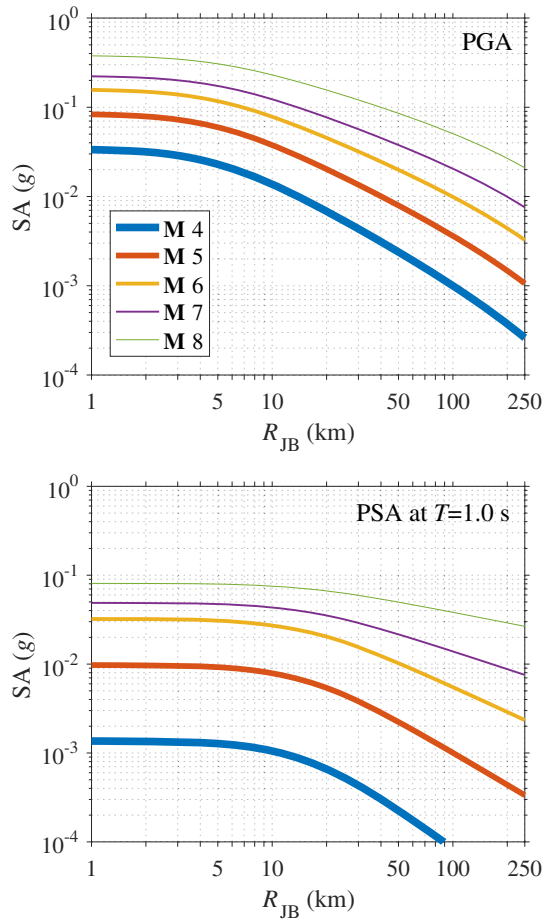


**Figure 8.** Comparison of distance scaling characteristics of our proposed GMPEs for the vertical component of spectral accelerations for a reference site with  $V_{S30} = 760$  m/s. The color version of this figure is available only in the electronic edition.

evaluation of these figures shows random distributions of residuals, indicating that there are no obvious biases, and no significant trends and models fit the observations well.

There are two approaches to develop vertical design spectra for a particular site: using vertical GMPEs or using the vertical-to-horizontal (V/H) ratio approach (Bommer *et al.*, 2011; Gülerce and Abrahamson, 2011). In this article, we developed GMPEs for the vertical component as well as for the horizontal component using a dataset of Iran. Bozorgnia and Campbell (2016b) explained how the horizontal and vertical GMPEs can be combined to generate a model for V/H ratios, if the user wishes to work with the V/H ratio in practice. The reader is referred to Bozorgnia and Campbell (2016b), their equations 5–12 for more discussion. In essence, the V/H ratio is a function of spectral period, source to site distance, and earthquake magnitude (Niazi and Bozorgnia, 1992; Bozorgnia *et al.*, 1995). V/H ratios estimated from the proposed GMPEs for sites with  $V_{S30}$  of 360 and 760 m/s located at Joyner–Boore distances of 10 and 100 km are shown in Figure 15. The two-thirds value underestimates the V/H ratio in short periods, particularly in near-source regions, whereas the V/H ratio is

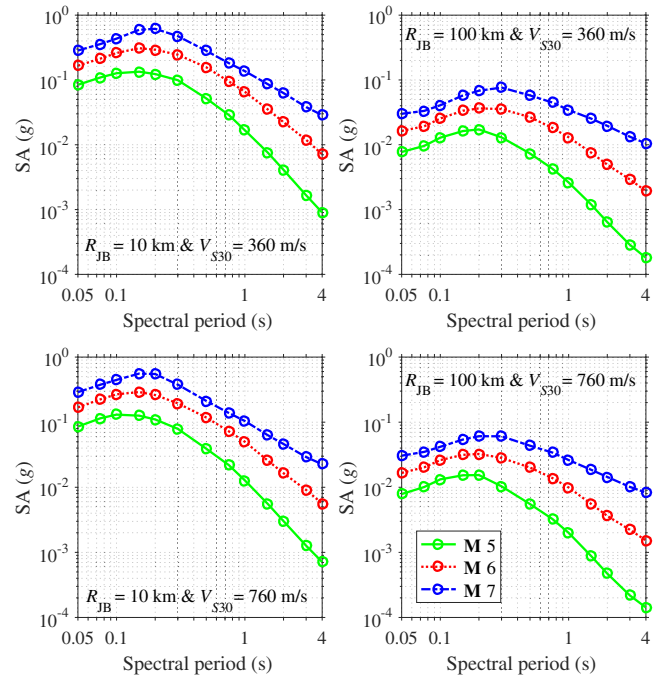


**Figure 9.** Variation of median estimates of response spectra versus spectral period for the horizontal component of spectral accelerations for sites with  $V_{S30}$  of 360 and 760 m/s at distances of 10 and 100 km. The color version of this figure is available only in the electronic edition.

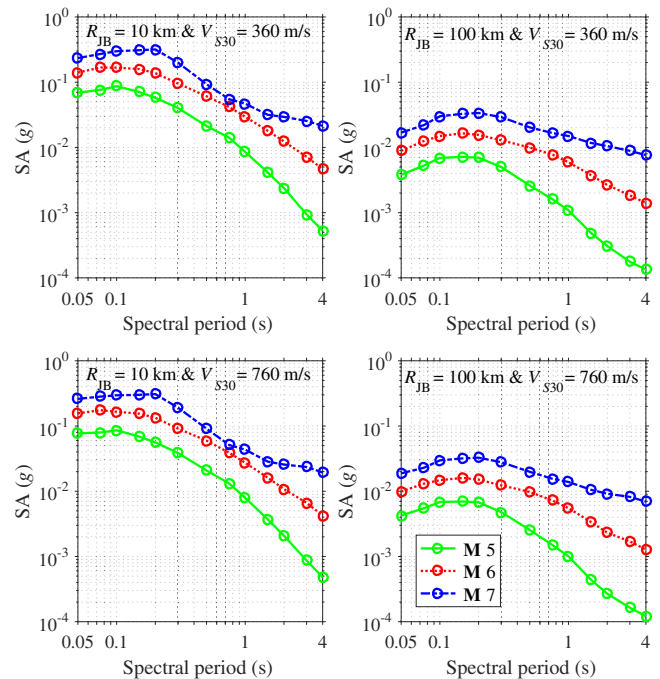


**Figure 10.** Variation of median estimates of response spectra versus spectral period for the vertical component of spectral accelerations for sites with  $V_{S30}$  of 360 and 760 m/s at distances of 10 and 100 km. The color version of this figure is available only in the electronic edition.

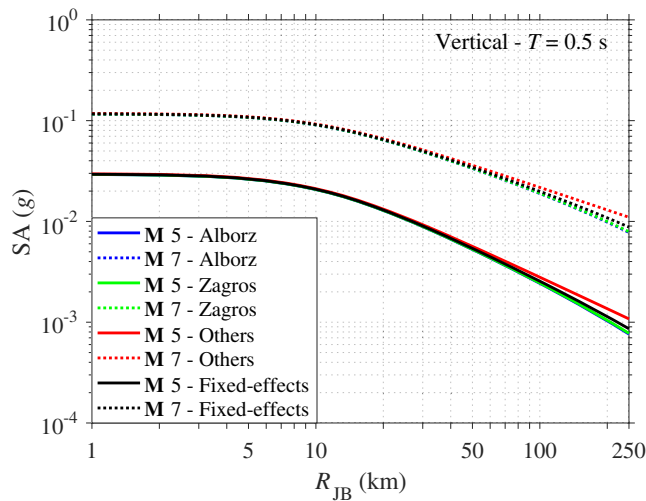


**Figure 11.** Effects of considering regional differences on the median prediction for the vertical component at  $T = 0.5$  s. The color version of this figure is available only in the electronic edition.

less than two-thirds at longer periods. It can be observed that as the Joyner–Boore distance gets shorter, the V/H spectral ratio increases. V/H ratios are high (near 1) at short periods and have peaks at 0.1 s for distances of 100 km, indicating the effects of the soil sites in which the horizontal motion is reduced at short periods (Bozorgnia and Campbell, 2016b), whereas the effects of soil sites on the vertical component is negligible. In the middle spectral period range, the V/H ratio is dropped, showing the stronger effect of the anelastic attenuation on the vertical motion.

### Summary and Conclusions

Increasing interest in performing region-specific and site-specific PSHA motivated us to develop new horizontal

GMPEs using a dataset from the Iranian strong ground motion database. Moreover, there are some limitations of V/H models discussed by Stewart *et al.* (2016). The last GMPEs for the vertical motions of Iranian records were developed over a decade ago in 2005. Therefore, in addition to deriving horizontal GMPEs, we directly developed vertical GMPEs, having a similar functional form to the horizontal direction, based on the vertical recorded strong ground motions. In this regard, we used a compiled dataset, which consists of 688 three-component accelerograms from 152 earthquakes. Our GMPEs are applicable to estimate horizontal and vertical ground-motion components of PGV (cm/s), PGA (g), and PSA (g) at spectral periods of 0.050–4.0 s. GMPEs were developed for active shallow crustal earthquakes within the Iranian plateau with moment magnitudes ranging from 4.7 to 7.4 and Joyner–Boore distances up to 250 km. For magnitudes outside this magnitude range and for regions outside of the Iranian plateau, usage should be handled with caution and checked for compatibility. The developed GMPEs can be utilized for sites with  $V_{S30}$  in the 300–1000 m/s range. Although the range of  $V_{S30}$  of stations used in the dataset varies from 155 to 1564 m/s, most of the stations have  $V_{S30}$  ranging from 300 to 1000 m/s.

The results obtained from this study are as follows:

- Eliminating the fault type term from the functional form reduced the total aleatory standard deviation by 10%.
- Site-to-site variability (see ⊕ Tables S7 and S8) is an important part of the total aleatory standard deviation. Removing this component from the total standard deviation and modeling it into the site-specific adjustment can significantly reduce the aleatory uncertainty.
- The apparent anelastic attenuation rate is faster for the vertical direction compared to the horizontal direction.

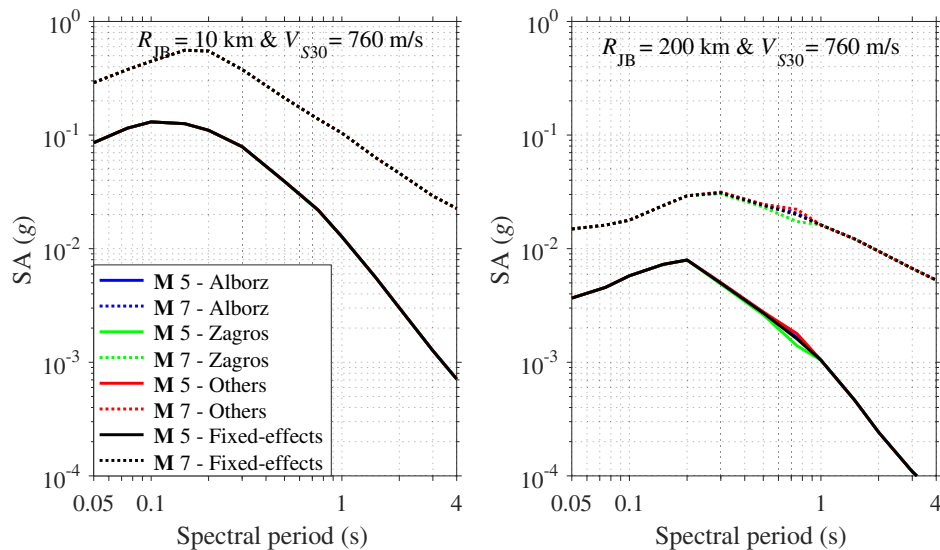


**Figure 12.** Effects of considering regional differences on response spectra for the horizontal component. The color version of this figure is available only in the electronic edition.

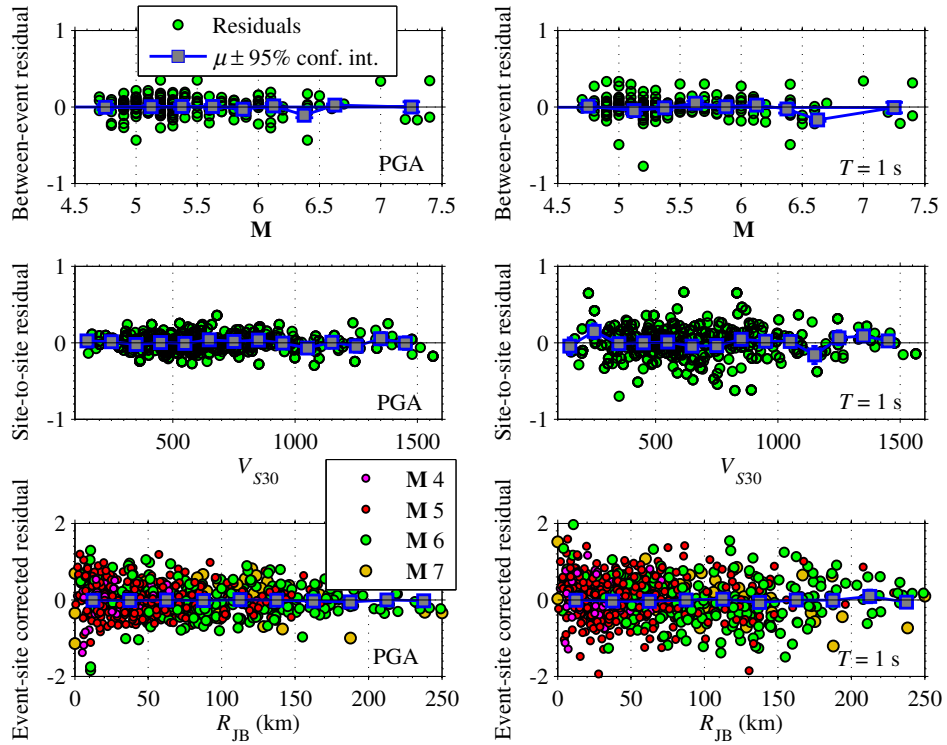


**Figure 13.** Distribution of between-event, site-to-site, and event-site corrected residuals (in natural logarithm units) for horizontal ground-motion components of PGA and PSA at spectral period 1.0 s. Error bars represent the mean and  $\pm 95\%$  confidence interval of the mean binned residuals. The color version of this figure is available only in the electronic edition.

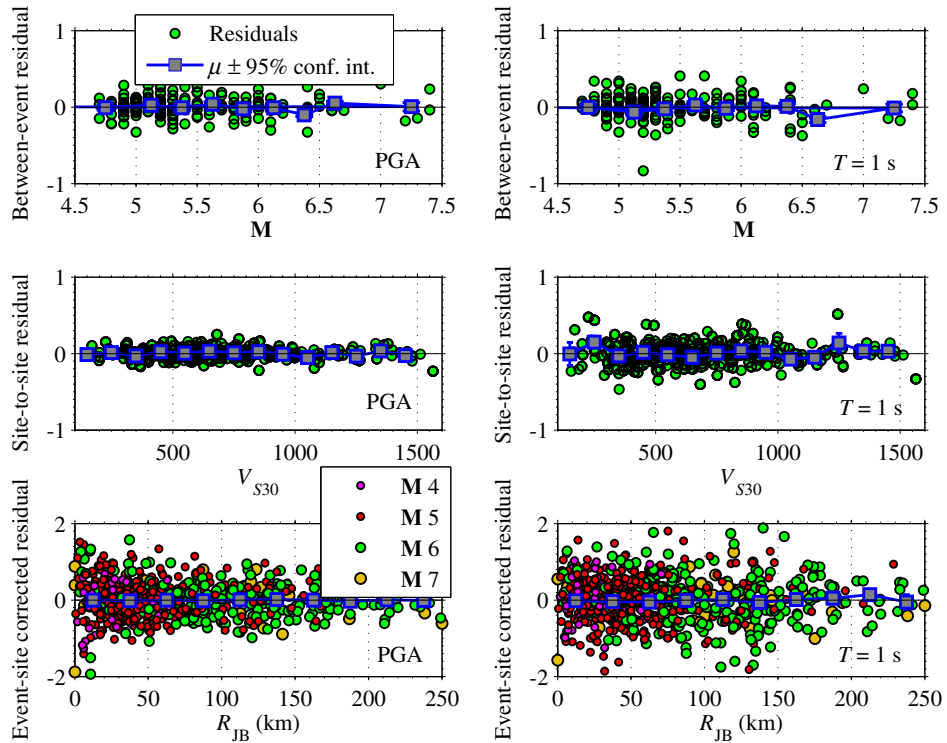


**Figure 14.** Distribution of between-event, site-to-site, and event-site corrected residuals (in natural logarithm units) for vertical ground-motion components of PGA and PSA at spectral period 1.0 s. Error bars represent the mean and  $\pm 95\%$  confidence interval of the mean binned residuals. The color version of this figure is available only in the electronic edition.

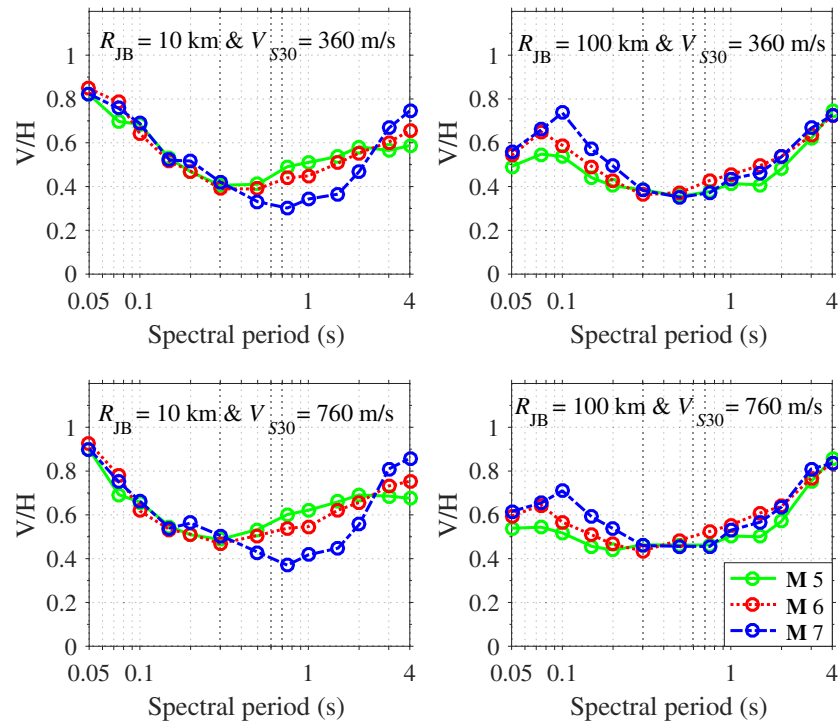


**Figure 15.** Vertical-to-horizontal (V/H) ratios dependency on moment magnitude ( $M$ ), distance ( $R_{JB}$ ), and  $V_{S30}$ . The color version of this figure is available only in the electronic edition.

- Site effects are negligible for the vertical direction, while having a significant effect for the horizontal direction.
- The predominant period increases with increasing magnitude on the horizontal direction, but it is fairly constant on the vertical direction.
- We observed regional variations only in the anelastic attenuation term, not in the site-response term. Allowing regional variations as random-effects coefficients inside the functional form affects long distances predictions, resulting in reduction of the total standard deviation.
- The analysis of residuals revealed that no trends were apparent and that the proposed GMPEs are generally unbiased with respect to the estimator parameters.

### Data and Resources

Strong ground motion records used in this study were provided by the Building and Housing Research Center (BHRC) of Iran ([www.bhrc.ac.ir](http://www.bhrc.ac.ir), last accessed September 2016).

### Acknowledgments

The authors are grateful to John Douglas, Thomas Pratt, Sreeram Reddy Kotha, Mehdi Zare, and an anonymous reviewer whose thoughtful comments and constructive suggestions significantly improved the article. We would also like to thank Yi-Hau Chen and Chu-Chuan Peter Tsai for providing us with their database and MATLAB codes.

### References

- Abrahamson, N. A., and R. R. Youngs (1992). A stable algorithm for regression analysis using the random effects model, *Bull. Seismol. Soc. Am.* **82**, 505–510.
- Aki, K. (1980). Attenuation of shear-waves in the lithosphere for frequencies from 0.05 to 25 Hz, *Phys. Earth Planet. In.* **21**, 50–60.
- Akkar, S., and J. J. Bommer (2006). Influence of long-period filter cut-off on elastic spectral displacements, *Earthq. Eng. Struct. Dynam.* **35**, 1145–1165.
- Akkar, S., and J. J. Bommer (2007). Empirical prediction equations for peak ground velocity derived from strong-motions records from Europe and the Middle East, *Bull. Seismol. Soc. Am.* **97**, 511–530.
- Al Atik, L., N. Abrahamson, J. J. Bommer, F. Scherbaum, F. Cotton, and N. Kuehn (2010). The variability of ground motion prediction models and its components, *Seismol. Res. Lett.* **81**, 794–801.
- Ambraseys, N. N., and J. Douglas (2003). Near-field horizontal and vertical earthquake ground motions, *Soil Dynam. Earthq. Eng.* **23**, no. 1, 1–18.
- Anderson, J. G., and J. N. Brune (1999). Probabilistic seismic hazard assessment without the ergodic assumption, *Seismol. Res. Lett.* **70**, 19–28.
- Anderson, J. G., and S. E. Hough (1984). A model for the shape of the Fourier amplitude spectrum of acceleration at high frequencies, *Bull. Seismol. Soc. Am.* **74**, 1969–1993.
- Ansari, A., and K. Amini Hosseini (2014). Broadband seismic network of Iran and increasing quality of seismic recordings, *Seismol. Res. Lett.* **85**, 878–888.
- Atkinson, G. M. (2004). Empirical attenuation of ground motion spectral amplitudes in southeastern Canada and the northwestern United States, *Bull. Seismol. Soc. Am.* **94**, 1079–1095.
- Atkinson, G. M. (2006). Single-station sigma, *Bull. Seismol. Soc. Am.* **96**, 446–455.
- Atkinson, G. M., and D. M. Boore (2014). The attenuation of Fourier amplitudes for rock sites in eastern North America, *Bull. Seismol. Soc. Am.* **104**, 513–528.

- Berberian, M., and A. Mohajer Ashjai (1977). Seismic risk map of Iran, a proposal, *Geol. Surv. Iran* **41**, 121–148.
- Berberian, M., and R. S. Yeats (1999). Patterns of historical earthquake rupture in the Iranian plateau, *Bull. Seismol. Soc. Am.* **89**, 120–139.
- Bindi, D., M. Massa, L. Luzi, G. Ameri, F. Pacor, R. Puglia, and P. Augliera (2014). Pan-European ground-motion prediction equations for the average horizontal component of PGA, PGV, and 5%-damped PSA at spectral periods up to 3.0 s using the RESORCE dataset, *Bull. Earthq. Eng.* **12**, 391–430.
- Bindi, D., F. Pacor, L. Luzi, R. Puglia, M. Massa, G. Ameri, and R. Paolucci (2011). Ground motion prediction equations derived from the Italian strong motion database, *Bull. Earthq. Eng.* **9**, 1899–1920.
- Bommer, J. J., S. Akkar, and O. Kale (2011). A model for vertical-to-horizontal response spectral ratios for Europe and the Middle East, *Bull. Seismol. Soc. Am.* **101**, 1783–1806.
- Boore, D. M., and J. J. Bommer (2005). Processing of strong-motion accelerograms: Needs, options and consequences, *Soil Dynam. Earthq. Eng.* **25**, 93–115.
- Boore, D. M., J. P. Stewart, E. Seyhan, and G. M. Atkinson (2014). NGA-West2 equations for predicting PGA, PGV, and 5% damped PSA for shallow crustal earthquakes, *Earthq. Spectra* **30**, 1057–1085.
- Boore, D. M., J. Watson-Lamprey, and N. A. Abrahamson (2006). Orientation-independent measures of ground motion, *Bull. Seismol. Soc. Am.* **96**, 1502–1511.
- Bozorgnia, Y., and K. W. Campbell (2004). Engineering characterization of ground motion, in *Earthquake Engineering: From Engineering Seismology to Performance-Based Engineering*, Y. Bozorgnia and V. V. Bertero (Editors), CRC Press, Boca Raton, Florida, 215–315.
- Bozorgnia, Y., and K. W. Campbell (2016a). Vertical ground motion model using NGA-West2 database, *Earthq. Spectra* **32**, 979–1004.
- Bozorgnia, Y., and K. W. Campbell (2016b). Vertical-to-horizontal (V/H) ground motion model, *Earthq. Spectra* **32**, 951–978.
- Bozorgnia, Y., M. Niazi, and K. W. Campbell (1995). Characteristics of free-field vertical ground motion during the Northridge earthquake, *Earthq. Spectra* **11**, 515–525.
- Chen, Y.-H., and C.-C. P. Tsai (2002). A new method for estimation of the attenuation relationship with variance components, *Bull. Seismol. Soc. Am.* **92**, 1984–1991.
- Douglas, J. (2004a). Use of analysis of variance for the investigation of regional dependence of strong ground motions, *13th World Conf. on Earthquake Engineering*, Vancouver, Canada, Paper No. 29.
- Douglas, J. (2004b). An investigation of analysis of variance as a tool for exploring regional differences in strong ground motions, *J. Seismol.* **8**, 485–496.
- Douglas, J., and D. M. Boore (2011). High-frequency filtering of strong-motion records, *Bull. Earthq. Eng.* **9**, 395–409.
- Elnashai, A., and A. Papazoglou (1997). Procedure and spectra for analysis of RC structures subjected to strong vertical earthquake loads, *J. Earthq. Eng.* **1**, 121–155.
- Ghasemi, H., M. Zare, and Y. Fukushima (2008). Ranking of several ground-motion models for seismic hazard analysis in Iran, *J. Geophys. Eng.* **5**, 301–310.
- Ghasemi, H., M. Zare, Y. Fukushima, and K. Koketsu (2009). An empirical spectral ground motion model for Iran, *J. Seismol.* **13**, 499–515.
- Ghodrati Amiri, G., M. Khorasani, M. Mirza Hessabi, and S. A. Razavian Amrei (2010). Ground motion prediction equations of spectral ordinates and Arias intensity for Iran, *J. Earthq. Eng.* **14**, 1–29.
- Ghodrati Amiri, G., A. Mahdavian, and F. M. Dana (2007). Attenuation relationships for Iran, *J. Earthq. Eng.* **11**, 469–492.
- Gülerce, Z., and N. A. Abrahamson (2011). Site-specific spectra for vertical ground motion, *Earthq. Spectra* **27**, 1023–1047.
- Hamzehloo, H., and M. Mahood (2012). Ground motion attenuation relationship for east central Iran, *Bull. Seismol. Soc. Am.* **102**, 2677–2684.
- Kaklamanos, J., and L. G. Baise (2011). Model validations and comparisons of the Next Generation Attenuation of Ground Motions (NGA-West) Project, *Bull. Seismol. Soc. Am.* **101**, 160–175.
- Kale, O., S. Akkar, A. Ansari, and H. Hamzehloo (2015). A ground-motion predictive model for Iran and Turkey for horizontal PGA, PGV, and 5% damped response spectrum: Investigation of possible regional effects, *Bull. Seismol. Soc. Am.* **105**, 963–980.
- Kotha, S. R., D. Bindi, and F. Cotton (2016). Partially non-ergodic region specific GMPE for Europe and Middle-East, *Bull. Earthq. Eng.* **14**, 1245–1263.
- Kotha, S. R., D. Bindi, and F. Cotton (2017). Towards a non-ergodic probabilistic seismic hazard assessment in Europe and Middle East, *16th World Conf. on Earthquake Engineering (16WCEE)*, Santiago, Chile, 9–13 January 2017.
- Kramer, S. L. (1996). *Geotechnical Earthquake Engineering*, Prentice-Hall, Inc., Upper Saddle River, New Jersey.
- Lermo, J., and F. Chavez-Garcia (1993). Site effect evaluation using spectral ratios with only one station, *Bull. Seismol. Soc. Am.* **83**, 1574–1594.
- Lindstrom, M. J., and D. M. Bates (1990). Nonlinear mixed effects models for repeated measures data, *Biometrics* **46**, 673–687.
- MathWorks Inc. (2015). *MATLAB and Statistics and Machine Learning Toolbox*, The MathWorks Inc., Natick, Massachusetts.
- Mousavi, M., A. Ansari, H. Zafarani, and A. Azarbakht (2012). Selection of ground motion prediction models for seismic hazard analyses in Zagros region, Iran, *J. Earthq. Eng.* **16**, 1184–1207.
- Niazi, M., and Y. Bozorgnia (1991). Behavior of near-source peak horizontal and vertical ground motions over SMART-1 array, Taiwan, *Bull. Seismol. Soc. Am.* **81**, 715–732.
- Niazi, M., and Y. Bozorgnia (1992). Behaviour of near-source vertical and horizontal response spectra at smart-1 array, Taiwan, *Earthq. Eng. Struct. Dynam.* **21**, 37–50.
- Nowroozi, A. A. (2005). Attenuation relations for peak horizontal and vertical accelerations of earthquake ground motion in Iran: A preliminary analysis, *J. Seismol. Earthq. Eng.* **7**, 109–128.
- Rezaeian, S., M. D. Petersen, and M. P. Moschetti (2015). Ground motion models used in the 2014 U.S. national seismic hazard maps, *Earthq. Spectra* **31**, S59–S84.
- Rodriguez-Marek, A., E. M. Rathje, J. J. Bommer, F. Scherbaum, and P. J. Stafford (2014). Application of single-station sigma and site-response characterization in a probabilistic seismic-hazard analysis for a new nuclear site, *Bull. Seismol. Soc. Am.* **104**, 1601–1619.
- Sadeghi, H., A. Shoostari, and M. Jaladat (2010). Prediction of horizontal response spectra of strong ground motions in Iran and its regions, *Proc. of the 9th U.S. National and 10th Canadian Conf. on Earthquake Engineering: Reaching Beyond Borders*, Toronto, Canada, 25–29 July, Paper Number 861.
- Saffari, H., Y. Kuwata, S. Takada, and A. Mahdavian (2012). Updated PGA, PGV, and spectral acceleration attenuation relations for Iran, *Earthq. Spectra* **28**, 257–276.
- Scherbaum, F., F. Cotton, and P. Smit (2004). On the use of response spectral reference data for the selection and ranking of ground-motion models for seismic hazard analysis in regions of moderate seismicity: The case of rock motion, *Bull. Seismol. Soc. Am.* **94**, 1–22.
- Scherbaum, F., E. Delavaud, and C. Riggelsen (2009). Model selection in seismic hazard analysis: An information theoretic perspective, *Bull. Seismol. Soc. Am.* **99**, 3234–3247.
- Sedaghati, F., and S. Pezeshk (2016a). Investigation of regional differences in strong ground motions for the Iranian plateau, *World Acad. Sci. Eng. Tech., Int. J. Environ. Chem. Ecol. Geol. Geophys. Eng.* **10**, no. 6, 591–594.
- Sedaghati, F., and S. Pezeshk (2016b). Comparative study on parameter estimation methods for attenuation relationships, *J. Geophys. Eng.* **13**, no. 6, 912–927.
- Sedaghati, F., and S. Pezeshk (2016c). Estimation of the coda-wave attenuation and geometrical spreading in the New Madrid seismic zone, *Bull. Seismol. Soc. Am.* **106**, no. 4, 1482–1498.
- Sella, G. F., H. T. Dixon, and A. Mao (2002). REVEL: A model for recent plate velocities from space geodesy, *J. Geophys. Res.* **107**, 11–30.

- Soghrat, M. R., and M. Ziyaeifar (2016). Ground motion prediction equations for horizontal and vertical components of acceleration in northern Iran, *J. Seismol.* **1**, 1–27, doi: [10.1007/s10950-016-9586-4](https://doi.org/10.1007/s10950-016-9586-4).
- Stafford, P. J. (2014). Crossed and nested mixed-effects approaches for enhanced model development and removal of the ergodic assumption in empirical ground-motion models, *Bull. Seismol. Soc. Am.* **104**, 702–719.
- Stewart, J. P., D. M. Boore, E. Seyhan, and G. M. Atkinson (2016). NGA-West2 equations for predicting vertical-component PGA, PGV, and 5%-damped PSA from shallow crustal earthquakes, *Earthq. Spectra* **32**, 1005–1031.
- Tavakoli, B., and M. Ghafory-Ashtiany (1999). Seismic hazard assessment of Iran, *Ann. Geophys.* **42**, 1013–1021.
- Tavakoli, B., and S. Pezeshk (2005). Empirical-stochastic ground-motion prediction for eastern North America, *Bull. Seismol. Soc. Am.* **95**, 2283–2296.
- Zafarani, H., and M. Mousavi (2014). Applicability of different ground-motion prediction models for northern Iran, *Nat. Hazards* **73**, 1199–1228.
- Zandieh, A., and S. Pezeshk (2011). A study of horizontal-to-vertical component spectral ratio in the New Madrid seismic zone, *Bull. Seismol. Soc. Am.* **101**, 287–296.
- Zare, M., and S. Sabzali (2006). Spectral attenuation of strong motions in Iran, *Proc. of Third International Symposium on the Effects of Surface Geology on Seismic Motion*, Grenoble, France, 30 August–1 September.

Department of Civil Engineering  
The University of Memphis  
3815 Central Avenue  
Memphis, Tennessee 38152  
fsdghati@memphis.edu  
spezeshk@memphis.edu

Manuscript received 27 June 2016;  
Published Online 7 February 2017